haematologica
Journal of the Ferrata Storti Foundation

A first-in-class Wiskott-Aldrich syndrome protein activator with anti-tumor activity in hematologic cancers

by Filippo Spriano, Giulio Sartori, Jacopo Sgrignani, Laura Barnabei, Alberto J. Arribas, Matilde Guala, Ana Maria Carrasco del Amor, Meagan R. Tomasso, Chiara Tarantelli, Luciano Cascione, Gaetanina Golino, Maria E. Riveiro, Roberta Bortolozzi, Antonio Lupia, Francesco Paduano, Samuel Huguet, Keyvan Rezai, Andrea Rinaldi, Francesco Margheriti, Pedro Ventura, Greta Guarda, Giosué Costa, Roberta Rocca, Alberto Furlan, Luuk M. Verdonk, Paolo Innocenti, Nathaniel I. Martin, Giampietro Viola, Christoph Driessen, Emanuele Zucca, Anastasios Stathis, Digvijay Gahtory, Maurits van den Nieuwboer, Beat Bornhauser, Stefano Alcaro, Francesco Trapasso, Susana Cristobal, Shae B. Padrick, Natalina Pazzi, Franco Cavalli, Andrea Cavalli, Eugenio Gaudio, and Francesco Bertoni

Received: December 31, 2022.
Accepted: June 7, 2024.

Citation: Filippo Spriano, Giulio Sartori, Jacopo Sgrignani, Laura Barnabei, Alberto J. Arribas, Matilde Guala, Ana Maria Carrasco del Amor, Meagan R. Tomasso, Chiara Tarantelli, Luciano Cascione, Gaetanina Golino, Maria E. Riveiro, Roberta Bortolozzi, Antonio Lupia, Francesco Paduano, Samuel Huguet, Keyvan Rezai, Andrea Rinaldi, Francesco Margheriti, Pedro Ventura, Greta Guarda, Giosué Costa, Roberta Rocca, Alberto Furlan, Luuk M. Verdonk, Paolo Innocenti, Nathaniel I. Martin, Giampietro Viola, Christoph Driessen, Emanuele Zucca, Anastasios Stathis, Digvijay Gahtory, Maurits van den Nieuwboer, Beat Bornhauser, Stefano Alcaro, Francesco Trapasso, Susana Cristobal, Shae B. Padrick, Natalina Pazzi, Franco Cavalli, Andrea Cavalli, Eugenio Gaudio, and Francesco Bertoni. A first-in-class Wiskott-Aldrich syndrome protein activator with anti-tumor activity in hematologic cancers.
Haematologica. 2024 June 20. doi: 10.3324/haematol.2022.282672 [Epub ahead of print]

A first-in-class Wiskott-Aldrich syndrome protein activator with anti-tumor activity in hematologic cancers

Filippo Spriano [1*], Giulio Sartori [1], Jacopo Sgrignani [2], Laura Barnabei [1], Alberto J. Arribas [1,3], Matilde Guala [4], Ana Maria Carrasco Del Amor [5], Meagan R. Tomasso [6], Chiara Tarantelli [1], Luciano Cascione [1,3], Gaetanina Golino [1,7], Maria E Riveiro [8], Roberta Bortolozzi [9,10], Antonio Lupia [7,11], Francesco Paduano [12,13], Samuel Huguet [14], Keyvan Rezai [14], Andrea Rinaldi [1], Francesco Margheriti [1], Pedro Ventura[2], Greta Guarda [2], Giosuè Costa [12], Roberta Rocca [12], Alberto Furlan [2], Luuk M. Verdonk [15], Paolo Innocenti [15], Nathaniel I. Martin [15], Giampietro Viola [9,10], Christoph Driessen [16], Emanuele Zucca [1,17], Anastasios Stathis [17], Digvijay Gahtory [18], Maurits van den Nieuwboer [18], Beat Bornhauser [19], Stefano Alcaro [12], Francesco Trapasso [12], Susana Cristobal [5,20], Shae B. Padrick [6], Natalina Pazzi [4], Franco Cavalli [1], Andrea Cavalli [2], Eugenio Gaudio [1*#], Francesco Bertoni [1,17#],

[1] Institute of Oncology Research, Faculty of Biomedical Sciences, USI, Bellinzona, Switzerland; [2]Institute of Research in Biomedicine, Faculty of Biomedical Sciences, USI, Bellinzona, Switzerland; [3] SIB Swiss Institute of Bioinformatics, Lausanne, Switzerland;[4] Chimete, Tortona, Italy; [5] Department of Biomedical and Clinical Sciences, Cell Biology, Medical Faculty, Linköping University, Linköping, Sweden; [6] Drexel University, College of Medicine, Department of Biochemistry and Molecular Biology, Philadelphia, PA, USA; [7]Department of Pharmacy, University of Napoli Federico II, Napoli, Italy; [8] Early Drug Development Group, Boulogne-Billancourt, France; [9]Department of Woman's and Child's Health, University of Padova, Italy; [10] Istituto di Ricerca Pediatrica IRP, Fondazione Città della Speranza, Padova, Italy; [11] Net4science Srl, Magna Graecia University of Catanzaro, Catanzaro, Italy; [21] University "Magna Græcia" of Catanzaro, Catanzaro, Italy; [13] Tecnologica Research Institute and Marrelli Health, Biomedical Section, Stem Cells and Medical Genetics Units, Crotone, Italy. [14] Institut Curie, Paris, France; [15] Biological Chemistry Group, Institute of Biology Leiden, Leiden University, Leiden, The Netherlands; [16] Kantosspital St Gallen, St Gallen, Switzerland; [17] Oncology Institute of Southern Switzerland, Ente Ospedaliero Cantonale, Bellinzona, Switzerland; [18] BIMINI Biotech B.V., Leiden, The Netherlands; [19] Children's Hospital Zurich, Zurich, Switzerland; [20] Ikerbasque, Basque Foundation for Sciences, Department of Department of Physiology, Faculty of Medicine and Nursing, University of the Basque Country, Spain.

*, equally contributed; #, co-corresponding authors

Running title

A first-in-class WASp activator in hematological cancers

Corresponding authors:

Dr. Eugenio Gaudio, Institute of Oncology Research, via Francesco Chiesa 5, 6500 Bellinzona, Switzerland. e-mail: eugaudio1976@gmail.com

Prof. Francesco Bertoni, Institute of Oncology Research, via Francesco Chiesa 5, 6500 Bellinzona, Switzerland. Phone: +41 58 666 7206; e-mail: francesco.bertoni@ior.usi.ch

Keywords

WASp; lymphoma; multiple myeloma; leukemia; Wiskott-Aldrich syndrome; cytoskeleton.

Funding

Swiss National Science Foundation (SNSF 31003A_163232/1) to FB; Eurostars Project E!2829 HEMATO-WASP to DG, MvdN and FB; Swiss National Science Foundation 310030_185185 to

GGu; ERA-NET Marine Biotechnology project CYANOBESITY that it is cofounding from FORMAS, Sweden grant nr. 2016-02004 (SC); the project GOLIATH that has received funding from the European Union's Horizon 2020 research and innovation programme under grant agreement No 825489 (SC); IKERBASQUE, Basque Foundation for Science (SC); Basque Government grant IT-971-16 (SC) and LiU MS Core facility.

Conflict of interest

The Foundation for the Institute of Oncology Research is the owner of the patent WO2019185117 on EG-011, in which Matilde Guala, Natalina Pazzi, Francesco Bertoni, Eugenio Gaudio are listed as co-inventors. BIMINI Biotech has licensed the patent WO2019185117. Anastasios Stathis: institutional research funds from Pfizer, MSD; Roche, Novartis, Amgen, Abbvie, Bayer, ADC Therapeutics, MEI Therapeutics, Philogen, Celestia. Astra Zeneca; travel grant from AbbVie and PharmaMar; consulting fee payed to institution from Jansen, Roche, Eli Lilly. Emanuele Zucca: institutional research funds from Celgene, Roche and Janssen; advisory board fees from Celgene, Roche, Mei Pharma, Astra Zeneca and Celltrion Healthcare; travel grants from Abbvie and Gilead; expert statements provided to Gilead, Bristol-Myers Squibb and MSD. Greta Guarda: research funds from *OM-Pharma, Meyrin, and IFM Therapeutics, Boston.* Digvijay Gahtory, Maurits van den Nieuwboer: employees of BIMINI Biotech. Francesco Bertoni: institutional research funds from ADC Therapeutics, Bayer AG, Cellestia, Helsinn, HTG Molecular Diagnostics, ImmunoGen, Menarini Ricerche, NEOMED Therapeutics 1, Nordic Nanovector ASA, Oncternal Therapeutics, Spexis AG; consultancy fee from Helsinn, Menarini, BIMINI Biotech; advisory board fees from Novartis; expert statements provided to HTG Molecular Diagnostics; travel grants from Amgen, Astra Zeneca, iOnctura.

The other Authors have nothing to disclose.

Acknowledgments

We thank Jan Burkhardt and Ed Williamson (University of Pennsylvania) for the gift of the conformationally specific WASp antibody, Michael K. Rosen and Lynda Doolittle (University of Texas, Southwestern Medical Center) for the WASp expression constructs, Silvia Jenni, Yi-Chien Tsai (Children's Hospital Zurich, Zurich, Switzerland) for their technical assistance.

Author's contributions

F.S., G.S., L.B., J.S., A.J.A., M.G., A.M.C.D.A., M.R.T., C.T., L.C., G.Go., R.B., M.R., S.H., K.R., F.M., G.Gu., G.V., C.D., B.B., S.B.P, N.P., E.G., P.V., A.F, L.M.V., P.I., N.I.M., D.G., M.v.d.N. performed experiments. F.S., E.G., N.I.M., F.B., developed the methodology. F.S., G.L., A.M.C.D.A., S.C., M.R., S.B.P, E.G., N.I.M., analyzed data. F.S., G.S., M.R.T., G.Gu., S.C., S.B.P, M.v.d.N. F.B., E.G., wrote and/or edited the paper. A.L., G.C., R.R., A.C., S.A., provide computational chemistry advice. F.P., E.Z., A.S., F.T., F.C., provide scientific advice. F.B., E.G., contributed to the conception or design of the study. All Authors approved the final version of the manuscript.

Data Sharing Statement

Gene expression data will be available in available at the National Center for Biotechnology Information (NCBI) Gene Expression Omnibus (GEO; http://www.ncbi.nlm.nih.gov/geo) database

.

Abstract

Hematological cancers are among the most common cancers in adults and children. Despite significant improvements in therapies, many patients still succumb to the disease. Therefore, novel therapies are needed. The Wiskott-Aldrich syndrome protein (WASp) family regulates actin assembly in conjunction with the Arp2/3 complex, a ubiquitous nucleation factor. WASp is expressed exclusively in hematopoietic cells and exists in two allosteric conformations: auto-inhibited or activated. Here, we describe the development of EG-011, a first-in-class small molecule activator of the WASp auto-inhibited form. EG-011 possesses *in vitro* and *in vivo* anti-tumor activity as a single agent in lymphoma, leukemia, and multiple myeloma, including models of secondary resistance to PI3K, BTK, and proteasome inhibitors. The *in vitro* activity was confirmed in a lymphoma xenograft. Actin polymerization and WASp binding was demonstrated using multiple techniques. Transcriptome analysis highlighted homology with drugs-inducing actin polymerization.

Introduction

Hematological cancers are among the most common cancers in adults and in children [1, 2]. Improvements in patient outcomes are due to the introduction of therapies against novel targets (for example, inhibitors of BTK, PI3K, BCL2 of EZH2) or drugs with novel mechanisms of action on already known targets (for example, anti-CD19 chimeric antigen receptor T-cells, antibody-drug conjugates, or bispecific antibodies) [3]. Despite access to these therapies and the improvements in the management of patients, still, too many individuals succumb due to the emergence of relapses frequently refractory to standard therapies [2].

The Wiskott-Aldrich Syndrome (WAS) gene is almost exclusively expressed in cells belonging to the hematopoietic lineage [4]. Alterations of its protein (WASp) through loss-of-function (LOF) or activating gain-of-function (GOF) mutations give rise to WAS and to X-linked neutropenia (XLN), respectively [5, 6]. In XLN, hyperactivated WASp causes increased actin polymerization, causing genomic instability and apoptosis in lymphocytes [7]. In WAS patients, depletion of WASp protein or activity disrupts actin polymerization in T cells [8]. WASp directly interacts with FYN [9] and BTK [10], which are proteins involved in B cell receptor and Toll-like receptor signaling [3]. B cells without functioning WASp have defective actin cytoskeletons with reduced motility and aggregates compared to normal B cells [11]. Deletion of WASp in B cells also leads to the production of autoantibodies and the development of autoimmunity, as in Wiskott-Aldrich syndrome patients [12], and *WAS* mutations are associated with the development of lymphomas in around 15% of cases [13]. The complexity of WASp regulation and functions is underlined by data in ALK-positive anaplastic large cell lymphoma (ALCL), reporting both an oncogenic [14] and a tumor-suppressive role for the protein [15]. These identify the protein as an oncogene and a tumor suppressor [15]. WASp belongs to a family of proteins that share the VCA (verprolin homology, central, acidic) motif in their C-terminal portion [16]. WASp and the other members of the family (N-WASP, WAVE/SCAR1,2 and 3, WASH, JMY, and WHAMM) are involved in the actin assembly and cytoskeleton reorganization, using their VCA domains to promote nucleation of actin filaments by the Arp2/3 complex [16]. The activity of WASp is regulated through a well-studied allosteric mechanism, wherein WASp exists in two allosteric conformations. In the first (autoinhibited) conformation, an N-terminal domain binds to and sequesters the C-terminal VCA domain in a fashion coupled to protein folding [17]. The autoinhibited form is then activated by the competitive binding of the small GTPase Cdc42 [18], of the phospholipid PtdIns(4,5)P2 [19] or phosphorylation [20]. Additional layers of regulation occur through the clustering of WASp molecules into high-potency complexes[21, 22].

Small molecules affecting WASp functions have been reported. The small molecule wiskostatin inhibits WASp by inducing folding of the GBD into its autoinhibited conformation, stabilizing WASp into its autoinhibited conformation[23]. Another reported compound (SMC#13) promotes WASp degradation and has anti-tumor activity in lymphoma and leukemia models [24]. Thus, small molecules may mimic the effects of WASp mutants and selectively lead to cell death in hematological lineages, indicating WASp as a new target not yet explored in the clinical setting.

Here, we describe the fortuitous identification of a first-in-class WASp activator (EG-011) with specific activity in various hematological malignancies.

Methods

Cell lines

Sixty-two cell lines derived from human and non-human lymphomas (Table S1) were cultured according to the recommended conditions. All media were supplemented with fetal bovine serum (10/20%), Penicillin-Streptomycin-Neomycin (~5,000 units penicillin, 5 mg streptomycin and 10 mg neomycin/mL, Sigma Aldrich, US) and L-glutamine (1%). Cell line identity was authenticated by short tandem repeat DNA profiling [25]. All the experiments were performed within one/two month from being thawed. Cell lines were periodically tested to confirm Mycoplasma negativity using the MycoAlert Mycoplasma Detection Kit (Lonza, Visp, Switzerland). Detailed methods for additional cell lines derived from solid tumors and leukemia are provided in Supplementary Materials and Methods.

Compounds

EG-011 and analogs were synthesized in our laboratories and by Chimete (Tortona, Italy) (See Results section and supplementary results section). Rituximab (Roche, Switzerland) was dissolved in a physiological solution at 10 mg/ml concentration. Additional anti-cancer agents were purchased from Selleckchem (TX, USA) and prepared in DMSO at the stock concentration of 100 mM.

MTT proliferation assay, cell cycle, apoptosis assay, and drug combinations

Full methods are provided in Supplementary Materials and Methods.

Patient-derived xenografts

Drug responses in ALL patient-derived xenografts (PDX) were analyzed as previously described [26]. Full methods are provided in Supplementary Materials and Methods.

Xenografts experiments

NOD-Scid (NOD.CB17-*Prkdcscid*/NCrHsd) mice maintenance and animal experiments were performed under institutional guidelines established for the Animal Facility and with study protocols approved by the local Cantonal Veterinary Authority (No. TI-20-2015). Full methods are in Supplementary Materials and Methods).

Primary healthy PBMCs

Peripheral blood was obtained from two healthy donors. Peripheral blood mononuclear cells (PBMCs) were isolated by Ficoll density-gradient centrifugation and then cultured in the presence of DMSO or EG-011 (two doses: 1 and 10 μM). After 24 and 48 hours, the percentage of apoptotic cells was determined by staining of the cells with Annexin V-FITC

Gene expression profiling

REC1 cell line was exposed to DMSO and to EG-011(500 nM) for 8 hours. Gene Expression Profiling (GEP) was done using the HumanHT-12 v4 Expression BeadChip (Illumina, San Diego, CA, USA). Data processing and statistical analysis were performed using R/Bioconductor [27], as

previously described [28]. Transcript mapping was based on HG19 using manufacturer-supplied annotation. Data were analyzed using the omics playground platform (https://bigomics.ch)

Kinase assay screenings

EG-011 was screened against 468 human kinases at a concentration of 1 μM using the KINOMEscan assay, which was ATP independent (Discoverx, CA, USA), and, at 0.1 and 1 μM concentrations, against 320 kinases by running a regular ATP-related assay (Wildtype-Profiler, ProQinase, Freiburg, Germany).

Thermal proteome profiling (TPP), Surface plasmon resonance (SPR) and nuclear magnetic resonance (NMR)

TTP experiments were performed as described in Franken et al. [29] with some modifications. TPP, SPR and NMR methods are in Supplementary Materials and Methods.

Functional WASp experiments and Pyrene actin assembly assays

Full methods are provided in Supplementary Materials and Methods.

Immunofluorescence

For immunofluorescence methods, we used the VL51 sensitive cell line since the REC1 cell line was not compatible with the attaching protocol used. Full methods are in Supplementary Materials and Methods.

Cellular and in vivo pharmacokinetic, metabolic stability

Full methods are in Supplementary Materials and Methods.

Analogue synthesis

Full methods are in Supplementary Materials and Methods.

Results

EG-011 is a novel small molecule

We modified the central scaffold of the US Food and Drug Administration (FDA) approved BTK inhibitor ibrutinib (Figure 1A), replacing its central scaffold with one selected from the Zinc12 library [30], and we named the new molecule EG-011. The latter contains an aromatic heterocyclic nucleus pyrido [3,2-d] pyrimidine-2,4 (1H, 3H) -dione instead of the ibrutinib aromatic heterocyclic nucleus 1H-pyrazolo [3,4-d] pyrimidin-4-amino. EG-011 also differed at the 4phenoxyphenyl substituent in position 3, replaced with the 4phenoxybenzyl in position 1, and the piperidine substituent in position 1, shifted to position 3. The changes aimed to obtain a novel and patentable drug-like small molecule, possibly maintaining the reactive regions of ibrutinib related to its drug-like properties. The synthetic route to EG-011 was distinct from ibrutinib (Figure 1B) and is reported in the supplementary results section.

EG-011 has anti-tumor activity only among hematological cancers

We tested the potential anti-tumor activity of EG-011 in a panel of 62 lymphoma cell lines derived from various histological subtypes. The dose-response curve and MTT cell proliferation assay were performed after 72 hours of treatment. EG-011 showed anti-lymphoma activity with a median IC_{50} of 2.25 µM (95% C.I. 1-5 µM) (Figure 2 A,B; Table S1). A higher activity was observed in 21 cell lines with a median IC_{50} of 250 nM (95% C.I. 40-600 nM). Among these there were 11 germinal center B cell (GCB) diffuse large B cell lymphomas (DLBCL) (sensitive n=11/21, resistant n=9/41, $p < 0.05$), four mantle cell lymphoma (MCL) (sensitive n=4/21, resistant n=6/41, p n.s.) and three marginal zone lymphoma (MZL) (sensitive n=3/21, resistant n=2/41, p n.s.).

No activity was observed in 11 acute leukemia cell lines (Figure S1). However, 7 out of 12 primary cells derived from acute lymphoblastic leukemia (ALL) were sensitive to EG-011 with IC_{50} values between 0.3-4.6 µM after 72 h of exposure. The remaining five displayed IC_{50} higher than 20 µM (Figure S2).

EG-011 did not show any anti-proliferative activity in a panel of 23 solid tumor cell lines (IC_{50} > 10 µM), with only one cell line (head and neck tumor) sensitive with IC_{50} of 3.5 µM (Figure S2).

Comparing the activity of EG-011 in lymphoma cell lines and solid tumors, it was clear that EG-011 has activity specifically among hematological cancers (Figure S1).

The observed anti-proliferative activity of EG-011 was characterized by induction of cell death rather than cell cycle arrest, as indicated by surface exposed Annexin V and the dose-dependent increase in sub-G0 component (20-55%) observed in two sensitive lymphoma cell lines (OCI-LY-19 and REC1) exposed to the compound (500 nM and 2 µM; 72 h) (Figure 2C, D; Figure S3). No cytotoxicity was seen in PBMCs from two healthy donors after treatment with EG-011 at 1 and 10 µM for 24 h and 48 h (Figure 2E).

EG-011 is active in cell lines with resistance to FDA-approved compounds.

We tested EG-011 in models of secondary resistance to FDA-approved PI3K and BTK inhibitors developed in our laboratory from splenic MZL cell lines [31-33]. The anti-tumor activity of EG-011 was maintained or even increased in the resistant cell lines, both in terms of IC_{50} and area under the curve (AUC). EG-011 was especially active in VL51 idelalisib-resistant cell lines compared to their parental counterparts (IC_{50} 100 nM / AUC 895.7 vs IC_{50} 500 nM / AUC 1,124). (Figure 3A, B; Figure S4A). To further assess the lack of cross-resistance with other anti-cancer agents, we tested EG-011 in various multiple myeloma (MM) models with acquired resistance to proteasome inhibitors [34-36] (Figure 3C, D, E, F, Figure S4B). The anti-tumor activity of EG-011 was maintained, and it even increased in MM resistant cells. Overall, the sensitivity to EG-011 was maintained equally in sensitive and resistant cell lines. The RPMI-8266 bortezomib resistant line showed an IC50 around 20 times lower (IC_{50} 500 nM / AUC 282783) and a 4-fold increase in sensitivity was observed in RPMI-8266 carfilzomib resistant cells (IC_{50} 2.5 µM / AUC 424,223) compared to parental cell lines (IC_{50} 10µM /AUC 582,681).

These data indicate that EG-011 was active after the development of resistance to different FDA-approved agents was acquired.

EG-011 has *in vivo* anti-lymphoma activity

The observed *in vitro* anti-tumor activity of EG-011 was confirmed *in vivo* using the REC1 MCL cell line in a mouse xenograft model. EG-011 was administered at 200 mg/kg once per day, 5 days per week, and compared to vehicle control. EG-011 delayed tumor growth (volume) versus control (Day 6, Day 7, Day 9, $p < 0.05$) and final tumor weight (Figure 4A, B). EG-011-treated tumors were 2.2-fold smaller than controls ($p < 0.001$). Treatments were well tolerated in mice without significant signs of toxicity. Throughout treatment, mice were well-conditioned with a body condition score [37] BC3 for all groups.

Differences in cellular uptake do not explain the lack of activity in solid tumors

We analyzed the cellular PK properties of EG-011 in sensitive and resistant cell lines to address whether the lack of activity of EG-011 in solid tumor models could be sustained by differences in the compound's intake and kinetics. The colorectal cancer cell line HCT-116 was used as a resistant model ($IC_{50} > 10$ µM) and the MCL cell line REC1 as a sensitive model. Cellular uptake of EG-011 was rapid (< 5 min) in both sensitive and resistant cell lines, with a mean concentration of 10-20 ng/ml every 10^6 cells (20-40 nM) after 6h exposure (Figure S5). Extracellular levels of EG-011 were stable from treatment initiation for up to 6h exposure (~50 ng/mL in both cell lines. We observed a ratio of ~5 between intracellular and extracellular concentrations in both cell lines. In addition, we did not observe an active drug ejection of EG-011 in HCT-116 cells (Figure S5). These data indicated that the lack of activity in solid tumors was due to neither a different cellular uptake nor a higher ejection of the compound.

Transcriptome changes due to EG-011

We exposed a sensitive cell line (REC1) to EG-011 and looked at the transcriptome changes after 8h (Table S2). We identified, among others, a downregulation in MYC targets, mitotic spindle assembly genes involved in actin filaments organization. Comparing the genes modulated by EG-011 with publicly available data of other drugs (L1000 [38] and GDSC [39]), the new small molecules behaved similarly to microtubule-stabilizing agents and HDAC inhibitors. Among the top correlated drugs there were indeed docetaxel and epothilone B (Figure S6; Table S3). Lymphoma and pro-survival genes such as CXCR5, NFKBID, and BCL2A1 were among the top downregulated genes.

EG-011 exhibits covalent behavior

EG-011 contains an acrylamide moiety, which has the potential to act as a covalent warhead. To probe whether EG-011 covalently modifies its target, we synthesized a structural analog of EG-011 wherein the reactive acrylamide group was replaced with the fully saturated propenamide (Figure S7A). In line with expectation, this analog demonstrated a significantly reduced activity in cell-based assays, especially in sensitive cell lines (Figure S7B). This finding supports a covalent mechanism of action for EG-011.

EG-011 is the first in class WASp activator

As mentioned above, EG-011 was designed by modifying the BTK inhibitor ibrutinib, however, its pattern of activity did not correlate with ibrutinib's activity (Figure S8), indicating that EG-011 did not act via inhibiting the kinase. To assess whether additional kinases were inhibited by the compound,

we performed two screenings. First, EG-011 (1 µM) was compared to DMSO with a competition-binding assay against 450 human kinases and disease-relevant mutants (KINOMEscan). Second, EG-011 (100 nM, 1 µM) was compared to DMSO with a radiometric protein kinase assay against 320 human kinases (PanQinase Activity Assay). No effect against any kinase was observed (Table S4), indicating that EG-011 was not a kinase inhibitor.

To identify possible EG-011 targets in an unbiased manner, we then applied the thermal proteome profiling (TPP) technique [29]. The latter relies on the principle that, when subjected to heat, proteins denature and become insoluble, while upon interactions with small molecules, proteins can change their thermal stability. TPP was used by applying label-free quantitative mass spectrometry, facilitating the analysis of the changes of the melting profile within a complex mixture or across an entire proteome in a single experiment. TPP was performed on proteins extracted from EG-011-treated REC-1 cells (10 µM) and the corresponding control with a vehicle. The analysis of the EG-011 protein interactions identified 48 potential protein targets, eight stabilized and 40 destabilized (Figure S9, Table S5). WASp was the most highly destabilized protein by EG-011 (Table S5, Figure 5A). Since the pattern of expression of WASp, expressed only in hematopoietic cells [40], was compatible with the observed activity exclusively in hematological cancers, we performed experiments to confirm WASp as the target of EG-011. The binding of WASp and EG-011 was investigated by surface plasmon resonance (SPR) and nuclear magnetic resonance (NMR). We used two constructs: the WH1 domain and the GBD-C region [41]. The results of the SPR binding experiments (Figure S10) indicated that EG-011 binds to the WH1 domain with a Kd of 110 µM. The binding to this protein region was validated and confirmed by NMR experiments, an orthogonal assay for SPR.

One of the main functions of WASp is regulating the actin filament nucleation activity of Arp2/3 complex [42]. Thus, we reconstituted *in vitro* actin assembly with WASp, Arp2/3 complex and pyrene-labeled actin. EG-011 addition accelerates actin polymerization compared to actin with arp2/3 complex and WASp only. The slope of the fitting line was 50-60% higher compared to actin only, meaning a faster increase in actin polymerization in the presence of EG-011 (Figure 5B). Most importantly, the EG-011 analog lacking the acrylamide group did not affect actin polymerization. This is consistent with a direct effect of EG-011 on actin polymerization mediated by WASp.

If EG-011 activates actin polymerization via WASp, we predicted that sensitive cells might show increased actin polymerization upon EG-011 treatment. We examined cellular actin filament distribution using imaging. Cell lines were stained with Alexa Fluor 488 phalloidin following treatment with EG-011 or DMSO vehicle for 4, 8, and 24 h (500 nM and 5 µM). A significant increase in actin polymerization was seen in EG-011 sensitive (VL51) and not in resistant (Z-138) cell lines at 4, 8, and 24 h (Figure 5 C; Figure S11). An increase in actin polymerization was seen as a general increase in fluorescence and an increase in the number of high-intensity filamentous actin spots but not as an increase in the average area of cells (Figure 5 D-E). Similarly, long-term treatments produced an upregulation of actin polymerization, as seen by FACS (Figure S12). No differences were seen in the baseline levels of F-actin between sensitive and resistant cell lines.

We hypothesized that baseline levels of WASp autoinhibited or activated forms differ between EG-011 sensitive and resistant cell lines. Thus, we stained sensitive (Mino, VL51) and resistant cells

(MAVER1, Z138, U2932) with a specific antibody recognizing a WASp epitope available only in its activated form [43]. We did not observe any differences in the baseline level of the activated form of WASp (Figure 5F).

After exposing a sensitive cell line (VL51) to DMSO or EG-011 for 8 h (500 nM and 5 μM), we stained it for activated WASp. There was a significant increase in active WASp after EG-011 treatment, consistent with the changes in actin filament intensity stemming directly from WASp activation (Figure 5G). Thus, while the baseline degree of WASp activation does not explain the difference between sensitive and resistant cells, EG-011 does promote WASp activation.

Finally, EG-011 was tested with wiskostatin, a WASp inhibitor stabilizing the protein in its autoinhibited state [23]. The concomitant treatment between EG-011 and wiskostatin showed an antagonistic effect in the cell lines tested, confirming an opposite mode of action and target competition of the two compounds (Figure S13).

EG-011 *in vitro* synergizes with anti-lymphoma agents

EG-011-containing drug combinations were tested in EG-011 sensitive DLBCL (OCI-LY-1, OCI-LY-8, TMD8) and MCL (REC1, MINO) cell lines. Combination partners included the anti-CD20 monoclonal antibody rituximab, the chemotherapeutic agent bendamustine, the BCL2 inhibitor venetoclax, the BTK inhibitor ibrutinib, and the immunomodulator lenalidomide, all FDA approved agents (Figure S14). Ibrutinib and lenalidomide were tested in MCL and ABC-DLBCL (TMD8), the lymphoma subtypes in which clinical responses are observed [3]. The synergism was assessed with the Chou-Talalay combination index and as potency and efficacy according to the MuSyC algorithm [44, 45]. Based on the Chou-Talalay index, EG-011 showed synergism (median CI<0.9) with all the tested compounds in all the cell lines. Based on potency and efficacy parameters, all the combinations tested showed overall additivity or even synergism in efficacy and, to a lesser extent, in potency, as highlighted by most of the points in the upper right part of the squares (Figure S14 B-C). EG-011, in combination with rituximab and ibrutinib, showed an effect that was in most of the cases beneficial in terms of efficacy. At the same time, the increase in potency was given only by the addition of rituximab and ibrutinib to EG-011 and not vice versa.

EG-011 pharmacokinetics properties

Based on the positive *in vitro* and *in vivo* results, we performed initial studies to define the drug-like properties of EG-011. We first studied its metabolic stability (Figure S15) by incubation with cryopreserved hepatocytes of multiple species (rate, mice, dog, human) at different time points (0, 30, 60, 90, and 120 min), followed by liquid chromatography-tandem mass spectrometry (LC-MS/MS). The positive control compound 7-ethoxycumarin (7-EC) was rapidly metabolized with $t_{1/2}$ of 11, 15, 13, and 15 min in human, dog, rat, and mice hepatocytes, respectively (Figure S15B). EG-011 had a differential metabolism rate across the different species, with rodents having a very rapid $t_{1/2}$, 5, and 8 min in rats and mice, respectively. In contrast, human and dog hepatocyte incubations indicated a $t_{1/2}$ of 85 and 49 min, respectively. Based on this analysis, we characterized the

metabolites formed after incubation with mice and human hepatocytes for 120 min using a Quadrupole-Trap (QTRAP) LC-MS/MS. As shown in Figure S16, glutathionation and di-oxygenation (followed by hydrogenation) at the unsaturated handle attached to the piperidine ring were identified as the major metabolites. We also characterized the *in vivo* distribution of EG-011 by measuring the pharmacokinetics in mice for two dosage routes – intraperitoneal (ip) and oral (po) (200 mg/kg; blood collected after 5, 15, 30 min, 1, 2, 4 and 6 h). The pharmacokinetic experiment revealed that, in mice, the maximum circulating concentration (C_{max}) of EG-011 was reached in 30 min after oral administration, indicating amenability to absorption *in vivo*. The $t_{1/2}$ was calculated as 30 min and 5 h for IP and PO routes, respectively (Figure S17).

Discussion

Here, we report the discovery of a novel first-in-class WASp activator, EG-011, with preclinical anti-tumor activity in lymphoma, leukemia, and MM. The compound demonstrated cytotoxic activity in one-third of 62 lymphoma cell lines. Cell lines belonging to the GCB-DLBCL, MZL and MCL were particularly sensitive to the treatment. The *in vitro* anti-tumor activity was confirmed in an *in vivo* experiment with an MCL xenograft, with no evidence of toxicity.

Using different approaches, we demonstrated that EG-011 targets WASp. WASp was initially identified in an unbiased screen by a change in thermal stability upon EG-011 addition, and a direct binding was confirmed via SPR and NMR experiments. EG-011 activated WASp in reconstituted Arp2/3 complex-dependent actin polymerization assays. WASp activation by EG-011 was confirmed in cells using conformational-specific antibodies and increased actin polymerization in sensitive cells. As previously mentioned, WASp is predominantly found in an autoinhibited closed conformation, and it is activated by competitive binding of the small GTPase Cdc42 [23]. The active conformation is more open and unstable, in line with the decreased stability of WASp after EG-011 treatment. Importantly, WASp expression is exclusive to blood cells, explaining EG-011's lack of activity in a panel of cell lines derived from the most common solid tumors.

Transcriptome profiling of lymphoma cells exposed to EG-011 strengthened WASp as the drug target. There was downregulation of MYC targets and transcripts involved in mitotic spindle assembly and upregulation of genes involved in actin filament organization. Most importantly, the drugs with the most similar gene expression signatures to EG-011 were taxanes and HDAC inhibitors. Indeed, both microtubule-stabilization induced by taxanes and actin acetylation by HDAC inhibitors can lead to actin polymerization and cytoskeleton reorganization, followed by cell death [46, 47], as seen when exposing cells to EG-011.

Although apparently conflicting, the anti-tumor activities described here with an activator of WASp and in published papers with a WASp inhibitor are in line with the observed increased apoptosis and impairments of lymphocytes in individuals carrying or LOF or GOF WASp mutations [7, 8, 11]. Due to the fundamental role of WASp in regulating the cytoskeleton and cell division in lymphocytes, cell death of blood cancer cells appears pharmacologically achievable with different classes of WASp-targeting agents.

WASp has an important role not only in B cells but also in T cells. WASp is known to be activated via T-cell receptor signaling pathways to induce actin cytoskeleton rearrangements [48]. Due to this WASp involvement in T-cell activation and the observed direct antitumor activity, EG-011 could also have a role in the tumor microenvironment, increasing T-cell capacity to kill tumor cells [49]. Future experiments using immune-competent mouse models will help to explore the possible immune regulatory role of EG-011.

EG-011 showed synergism or additivity with rituximab, bendamustine, venetoclax, ibrutinib, and lenalidomide, indicating its potential use with other drugs. Finally, sensitivity to EG-011 was maintained in cells with acquired resistance to other agents. EG-011 was similarly active in splenic MZL cells before and after developing resistance to PI3K and BTK inhibitors. In MM, EG-011 was more active in the cells that had become resistant to proteasome inhibitors than in their parental counterparts.

Through modification of the reactive acrylamide group, we have demonstrated that EG-011 could exert a covalent activity, as confirmed by the loss of activity upon removal of the acrylamide group and the loss of the ability to induce actin polymerization.

In conclusion, EG-011 is a first-in-class activator of the WASp auto-inhibited conformation displaying anti-tumor activity in lymphoma, leukemia, and MM models. The data provide the rationale to explore this mechanism of action in hematological malignancies further.

References

1. Siegel RL, Giaquinto AN, Jemal A. Cancer statistics, 2024. CA Cancer J Clin. 2024;74(1):12-49.
2. Armitage JO, Gascoyne RD, Lunning MA, Cavalli F. Non-Hodgkin lymphoma. Lancet. 2017;390(10091):298-310.
3. Younes A, Ansell S, Fowler N, et al. The landscape of new drugs in lymphoma. Nat Rev Clin Oncol. 2017;14(6):335-346.
4. Kurisu S, Takenawa T. The WASP and WAVE family proteins. Genome Biol. 2009;10(6):226.
5. Massaad MJ, Ramesh N, Geha RS. Wiskott-Aldrich syndrome: a comprehensive review. Ann N Y Acad Sci. 2013;1285:26-43.
6. Keszei M, Record J, Kritikou JS, et al. Constitutive activation of WASp in X-linked neutropenia renders neutrophils hyperactive. J Clin Invest. 2018;128(9):4115-4131.
7. Westerberg LS, Meelu P, Baptista M, et al. Activating WASP mutations associated with X-linked neutropenia result in enhanced actin polymerization, altered cytoskeletal responses, and genomic instability in lymphocytes. J Exp Med. 2010;207(6):1145-1152.
8. Kenney D, Cairns L, Remold-O'Donnell E, Peterson J, Rosen FS, Parkman R. Morphological abnormalities in the lymphocytes of patients with the Wiskott-Aldrich syndrome. Blood. 1986;68(6):1329-1332.
9. Banin S, Truong O, Katz DR, Waterfield MD, Brickell PM, Gout I. Wiskott-Aldrich syndrome protein (WASp) is a binding partner for c-Src family protein-tyrosine kinases. Curr Biol. 1996;6(8):981-988.
10. Sakuma C, Sato M, Takenouchi T, Kitani H. Specific binding of the WASP N-terminal domain to Btk is critical for TLR2 signaling in macrophages. Mol Immunol. 2015;63(2):328-336.
11. Westerberg L, Larsson M, Hardy SJ, Fernandez C, Thrasher AJ, Severinson E. Wiskott-Aldrich syndrome protein deficiency leads to reduced B-cell adhesion, migration, and homing, and a delayed humoral immune response. Blood. 2005;105(3):1144-1152.
12. Shimizu M, Nikolov NP, Ueno K, et al. Development of IgA nephropathy-like glomerulonephritis associated with Wiskott-Aldrich syndrome protein deficiency. Clin Immunol. 2012;142(2):160-166.
13. Sullivan KE, Mullen CA, Blaese RM, Winkelstein JA. A multiinstitutional survey of the Wiskott-Aldrich syndrome. J Pediatr. 1994;125(6 Pt 1):876-885.
14. Murga-Zamalloa CA, Mendoza-Reinoso V, Sahasrabuddhe AA, et al. NPM-ALK phosphorylates WASp Y102 and contributes to oncogenesis of anaplastic large cell lymphoma. Oncogene. 2017;36(15):2085-2094.
15. Menotti M, Ambrogio C, Cheong TC, et al. Wiskott-Aldrich syndrome protein (WASP) is a tumor suppressor in T cell lymphoma. Nat Med. 2019;25(1):130-140.
16. Pollitt AY, Insall RH. WASP and SCAR/WAVE proteins: the drivers of actin assembly. J Cell Sci. 2009;122(Pt 15):2575-2578.
17. Luan Q, Zelter A, MacCoss MJ, Davis TN, Nolen BJ. Identification of Wiskott-Aldrich syndrome protein (WASP) binding sites on the branched actin filament nucleator Arp2/3 complex. Proc Natl Acad Sci U S A. 2018;115(7):E1409-E1418.
18. Kim AS, Kakalis LT, Abdul-Manan N, Liu GA, Rosen MK. Autoinhibition and activation mechanisms of the Wiskott-Aldrich syndrome protein. Nature. 2000;404(6774):151-158.
19. Higgs HN, Pollard TD. Activation by Cdc42 and PIP(2) of Wiskott-Aldrich syndrome protein (WASp) stimulates actin nucleation by Arp2/3 complex. J Cell Biol. 2000;150(6):1311-1320.
20. Cory GO, Cramer R, Blanchoin L, Ridley AJ. Phosphorylation of the WASP-VCA domain increases its affinity for the Arp2/3 complex and enhances actin polymerization by WASP. Mol Cell. 2003;11(5):1229-1239.
21. Padrick SB, Cheng HC, Ismail AM, et al. Hierarchical regulation of WASP/WAVE proteins. Mol Cell. 2008;32(3):426-438.
22. Padrick SB, Rosen MK. Physical mechanisms of signal integration by WASP family proteins. Annu Rev Biochem. 2010;79:707-735.
23. Peterson JR, Bickford LC, Morgan D, et al. Chemical inhibition of N-WASP by stabilization of a native autoinhibited conformation. Nat Struct Mol Biol. 2004;11(8):747-755.
24. Biber G, Ben-Shmuel A, Noy E, et al. Targeting the actin nucleation promoting factor WASp provides a therapeutic approach for hematopoietic malignancies. Nat Commun. 2021;12(1):5581.
25. Gaudio E, Tarantelli C, Spriano F, et al. Targeting CD205 with the antibody drug conjugate MEN1309/OBT076 is an active new therapeutic strategy in lymphoma models. Haematologica. 2020;105(11):2584-2591.

26. Frismantas V, Dobay MP, Rinaldi A, et al. Ex vivo drug response profiling detects recurrent sensitivity patterns in drug-resistant acute lymphoblastic leukemia. Blood. 2017;129(11):e26-e37.
27. Gentleman R, Carey V, Huber W, Irizarry R, Dudoit S. (eds) Bioinformatics and Computational Biology Solutions using R and Bioconductor. New York, NY, USA: Springer, 2005.
28. Spriano F, Chung EYL, Gaudio E, et al. The ETS Inhibitors YK-4-279 and TK-216 Are Novel Antilymphoma Agents. Clin Cancer Res. 2019;25(16):5167-5176.
29. Franken H, Mathieson T, Childs D, et al. Thermal proteome profiling for unbiased identification of direct and indirect drug targets using multiplexed quantitative mass spectrometry. Nat Protoc. 2015;10(10):1567-1593.
30. Irwin JJ, Sterling T, Mysinger MM, Bolstad ES, Coleman RG. ZINC: a free tool to discover chemistry for biology. J Chem Inf Model. 2012;52(7):1757-1768.
31. Arribas AJ, Napoli S, Cascione L, et al. ERBB4-Mediated Signaling Is a Mediator of Resistance to PI3K and BTK Inhibitors in B-cell Lymphoid Neoplasms. Mol Cancer Ther. 2024;23(3):368-380.
32. Arribas AJ, Napoli S, Gaudio E, et al. Abstract A127: Secretion of IL16 is associated with resistance to ibrutinib in pre-clinical models of lymphoma. Mol Cancer Ther. 2019;18(12_Supplement):A127-A127.
33. Arribas AJ, Napoli S, Cascione L, et al. Resistance to PI3Kdelta inhibitors in marginal zone lymphoma can be reverted by targeting the IL-6/PDGFRA axis. Haematologica. 2022;107(11):2685-2697.
34. Besse A, Stolze SC, Rasche L, et al. Carfilzomib resistance due to ABCB1/MDR1 overexpression is overcome by nelfinavir and lopinavir in multiple myeloma. Leukemia. 2018;32(2):391-401.
35. Besse L, Besse A, Mendez-Lopez M, et al. A metabolic switch in proteasome inhibitor-resistant multiple myeloma ensures higher mitochondrial metabolism, protein folding and sphingomyelin synthesis. Haematologica. 2019;104(9):e415-e419.
36. Brünnert D, Kraus M, Stühmer T, et al. Novel cell line models to study mechanisms and overcoming strategies of proteasome inhibitor resistance in multiple myeloma. Biochim Biophys Acta Mol Basis Dis. 2019;1865(6):1666-1676.
37. Ullman-Culleré MH, Foltz CJ. Body condition scoring: a rapid and accurate method for assessing health status in mice. Lab Anim Sci. 1999;49(3):319-323.
38. Musa A, Tripathi S, Dehmer M, Emmert-Streib F. L1000 Viewer: A Search Engine and Web Interface for the LINCS Data Repository. Front Genet. 2019;10:557.
39. Yang W, Soares J, Greninger P, et al. Genomics of Drug Sensitivity in Cancer (GDSC): a resource for therapeutic biomarker discovery in cancer cells. Nucleic Acids Res. 2012;41(Database issue):D955-D961.
40. Munoz P, Toscano MG, Real PJ, et al. Specific marking of hESCs-derived hematopoietic lineage by WAS-promoter driven lentiviral vectors. PLoS One. 2012;7(6):e39091.
41. Leung DW, Morgan DM, Rosen MK. Biochemical properties and inhibitors of (N-)WASP. Methods Enzymol. 2006;406:281-296.
42. Zigmond SH. How WASP regulates actin polymerization. J Cell Biol. 2000;150(6):F117-120.
43. Labno CM, Lewis CM, You D, et al. Itk functions to control actin polymerization at the immune synapse through localized activation of Cdc42 and WASP. Curr Biol. 2003;13(18):1619-1624.
44. Chou TC. Drug combination studies and their synergy quantification using the Chou-Talalay method. Cancer Res. 2010;70(2):440-446.
45. Meyer CT, Wooten DJ, Paudel BB, et al. Quantifying Drug Combination Synergy along Potency and Efficacy Axes. Cell Syst. 2019;8(2):97-108.
46. Rosenblum MD, Shivers RR. 'Rings' of F-actin form around the nucleus in cultured human MCF7 adenocarcinoma cells upon exposure to both taxol and taxotere. Comp Biochem Physiol C Toxicol Pharmacol. 2000;125(1):121-131.
47. Ong MS, Deng S, Halim CE, et al. Cytoskeletal Proteins in Cancer and Intracellular Stress: A Therapeutic Perspective. Cancers (Basel). 2020;12(1):238.
48. Malinova D, Fritzsche M, Nowosad CR, et al. WASp-dependent actin cytoskeleton stability at the dendritic cell immunological synapse is required for extensive, functional T cell contacts. J Leukoc Biol. 2016;99(5):699-710.
49. Kritikou JS, Oliveira MM, Record J, et al. Constitutive activation of WASp leads to abnormal cytotoxic cells with increased granzyme B and degranulation response to target cells. JCI Insight. 2021;6(6):e140273.

Online Supplementary Tables 1-5 provided as Excel files 1-5.

Figure Legends

Figure 1. EG-011 chemical structure and synthetic route. A, EG-011 chemical structure; **B**, Structural modifications between ibrutinib and EG-011. **C**, Synthetic route of EG-011.

Figure 2. EG-011 has strong in vitro anti-lymphoma activity. **A**, *In vitro* cell proliferation assay, represented as IC_{50}s calculated after 72 h of treatment, in 62 lymphoma cell lines. Cell lines are colored differently based on the different histological subtype. On the right, a representative dose response curve in one sensitive and one resistant cell line. **B**, IC50s distribution after EG-011 treatment among the different subtypes of lymphoma. Every dot represents one cell line with the respective IC50. Numbers on the bottom represents the number of cell lines present in each subtype group **C**, Percentage of apoptotic cells by annexin V staining after 48 or 72 h EG-011 treatment (100, 500 nM). Average and SD of at least two independent experiments**. D**, Cell cycle changes after 72 h EG-011 treatment (500 nM and 2 µM) in two sensitive lymphoma cell lines. Average and SD of at least two independent experiments. **E**, Percentage of apoptotic cells by annexin V after EG-011 treatment at 24 and 48 h in two primary cells from healthy control patients. * p-value < 0.05; **, p-value <0.0001

Figure 3. EG-011 is active in in models of secondary resistance to FDA approved compounds derived from splenic marginal zone lymphoma (A-B) and from multiple myeloma (C-F). Dose response curve after 72 h EG-011 treatment in cell lines with acquired resistance to FDA-approved compounds compared to parental cell lines. Splenic marginal zone lymphoma cell lines: **A**, VL51, parental, resistant to idelalisib, ibrutinib, or copanlisib; **B**, Karpas1718 parental or resistant to idelalisib. Multiple myeloma cell lines: **C**, AMO-1; **D**, L363; **E**, ARH77; **F**, RPMI-8226 parental, resistant to proteasome inhibitors carfilzomib (CFZ) and bortezomib (BTZ).

Figure 4. EG-011 has *in vivo* anti-lymphoma activity. A, *in vivo* activity of EG-011 (200 mg/Kg, IP, no.= 10 mice) compared to control vehicle (IP, no.= 9 mice) in NOD-SCID mice. The upper graph represents the mean tumor volume (mm^3) with standard error mean (SEM) for each day. The lower graph represents the growth of each individual animal under the control vehicle or EG-011 treatment. **B**, Tumor weights (mg) of control and EG-011 treated mice at the end of the treatment (day 9). P-values are calculated with the Mann-Whitney test. * p-value < 0.05; ***, p-value <0.0001.

Figure 5. EG-011 is the first-in-class WASp activator. A) Melting curves of WASP under DMSO (dashed lines) or EG-011 (solid lines) treatment. Protein lysate from an EG-011 sensitive cell line (REC1) was subjected to the thermal shift assay performed at temperatures between 37 °C to 67 °C in the presence or absence (vehicle) of EG-011. The unfolding profile shows a high decrease of solubility of WASp protein in the presence of EG-011 vs. vehicle. The melting temperature is shown with an "X" for each melting curve. Two biological replicates. **B)** Pyrene actin polymerization measured as fluorescence intensity. EG-011 was compared to actin only, actin plus Arp2/3 complex and Wasp, and the negative control LV009. Data are displayed as normalized fluorescence with SEM. Average of at least two independent experiments. **C)** Representative confocal images of sensitive lymphoma cell lines treated for 8h with DMSO or EG-011 (500 nM and 5 µM). Quantification of mean fluorescence intensity (ImageJ) per cell line in a 20X image (Leica widefield microscope) with n of around 200 cells. Experiments were performed in at least duplicate. Cells were stained for actin filament using Alexa Fluor™ 488-labeled phalloidin (green channel). Cells were counter-stained with DAPI (Blue channel).
D) Phalloidin Mean fluorescence intensity after EG-011 treatment (500 nM and 5 µM) at 3 time points (4, 8 and 24h) compared to DMSO in the sensitive cell line. The Kruskal-Wallis test, followed by Dunn's multiple comparisons, was performed. **E)** Number of high fluorescence intensity spots in a sensitive lymphoma cell line after EG-011 treatment (500 nM and 5 µM) at 3-time points (4, 8, and 24h) compared to DMSO. Cells are stained with phalloidin for filamentous actin (F-actin) visualization. Ratio pared T-test was performed **F)** Baseline levels of active WASP in sensitive and resistant cell lines. Cells are stained with antibody recognizing the active form of WASP. **G)** Increased levels of active WASP after 8h of EG-011 treatment (500 nM and 5 µM). All experiments are performed in at least duplicate. The Kruskal-Wallis test, followed by Dunn's multiple comparisons, was performed. Ns = nonsignificant; * p>0.05; **p<0.01; ***p<0.001; ****p<0.0001

A)

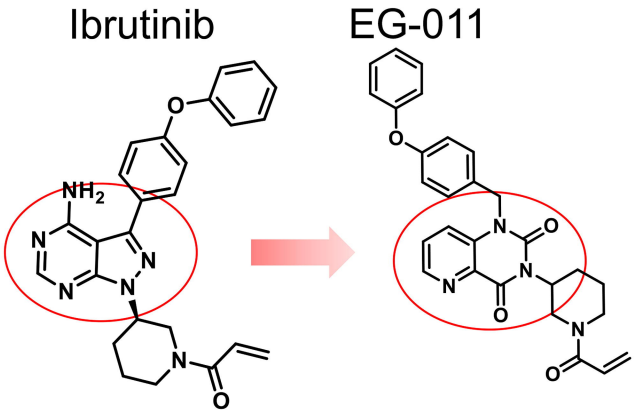
Ibrutinib
EG-011

B)

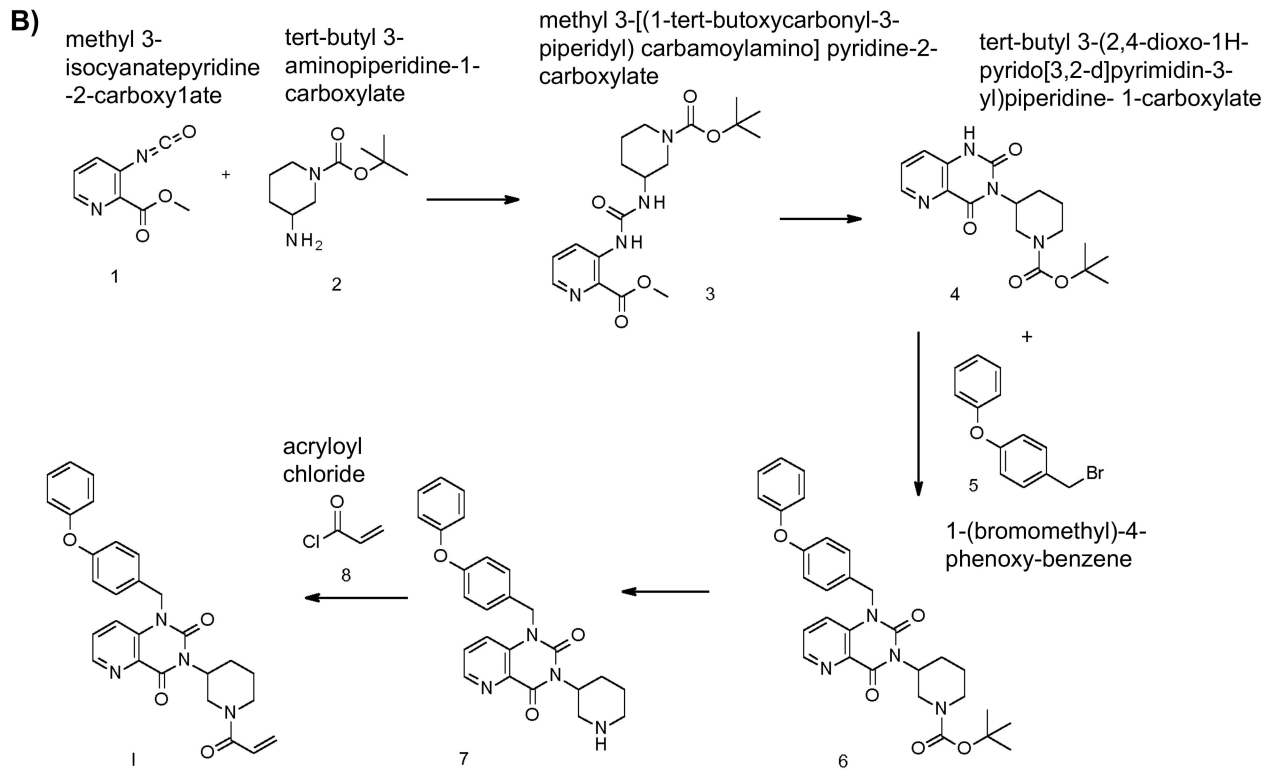
methyl 3-isocyanatepyridine-2-carboxy1ate
tert-butyl 3-aminopiperidine-1-carboxylate
methyl 3-[(1-tert-butoxycarbonyl-3-piperidyl) carbamoylamino] pyridine-2-carboxylate
tert-butyl 3-(2,4-dioxo-1H-pyrido[3,2-d]pyrimidin-3-yl)piperidine- 1-carboxylate
1
2
3
4
5
1-(bromomethyl)-4-phenoxy-benzene
acryloyl chloride
8
I
7
6
1-[(4-phenoxyphenyl)methyl]-3-(1-prop-2-enoyl-3-piperidyl)pyrido[3,2-d]pyrimidine-2,4-dione
1-[(4-phenoxyphenyl)methyl]-3-(3-piperidyl)pyrido[3,2-d]pyrimidine-2,4-dione
tert-butyl 3-[2,4-dioxo-1-[(4-phenoxyphenyl) methyl]pyrido[3,2-d]pyrimidin-3-yl]piperidine-1-carboxylate.

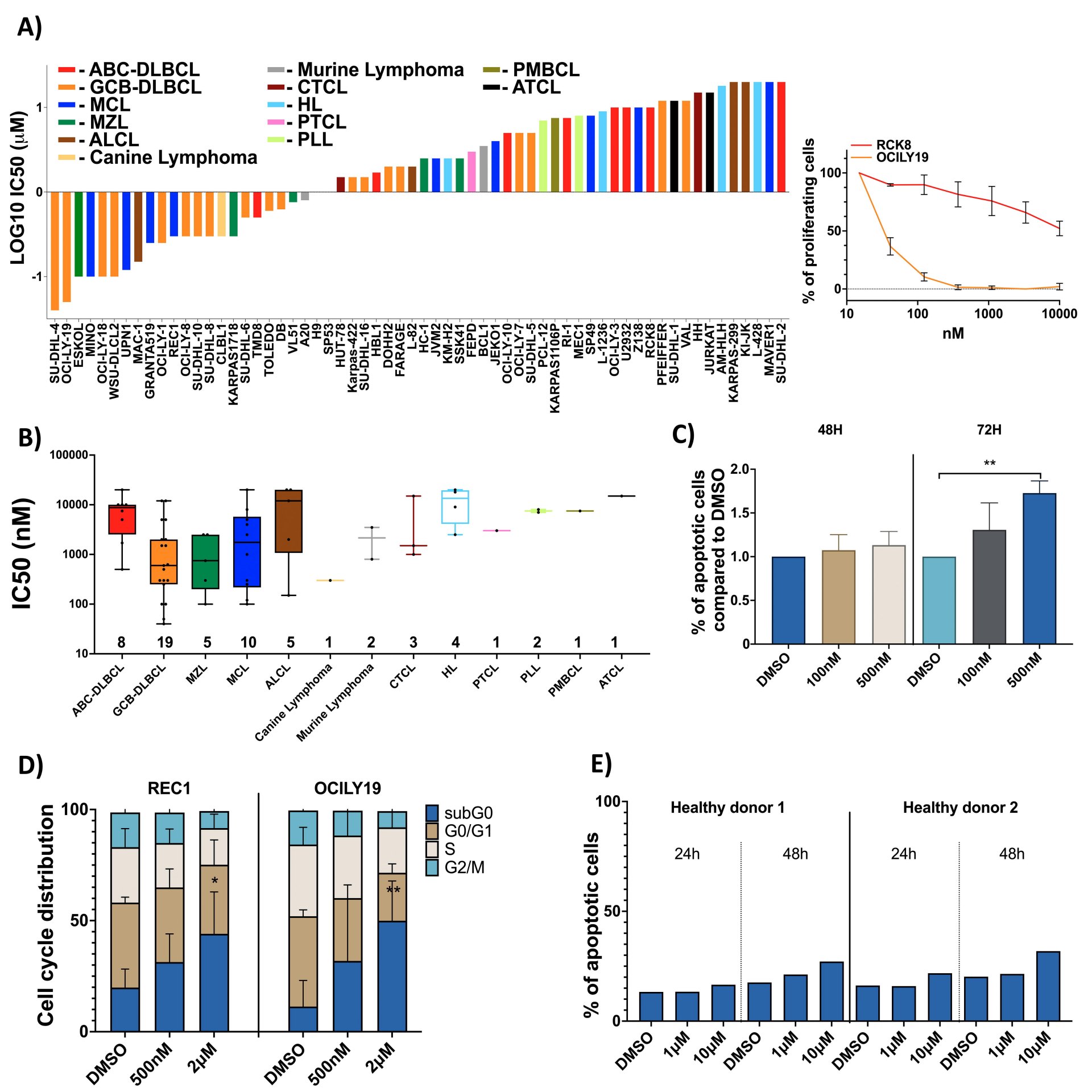
A)
- ABC-DLBCL
- GCB-DLBCL
- MCL
- MZL
- ALCL
- Canine Lymphoma
- Murine Lymphoma
- CTCL
- HL
- PTCL
- PLL
- PMBCL
- ATCL
LOG10 IC50 (μM)
SU-DHL-4 OCI-LY-19 ESKOL MINO OCI-LY-18 WSU-DLCL2 UPN1 MAC-1 GRANTA519 OCI-LY-1 REC1 OCI-LY-8 SU-DHL-10 SU-DHL-8 CLBL1 KARPAS1718 SU-DHL-6 TMD8 TOLEDO DB VL51 A20 H9 SP53 HUT-78 Karpas-422 SU-DHL-16 HBL1 DOHH2 FARAGE L-82 HC-1 JVM2 KM-H2 SSK41 FEPD BCL1 JEKO1 OCI-LY-10 OCI-LY-7 SU-DHL-5 PCL-12 KARPAS1106P RI-1 MEC1 SP49 L-1236 OCI-LY-3 U2932 Z138 RCK8 PFEIFFER SU-DHL-1 VAL HH JURKAT AM-HLH KARPAS-299 KI-JK L-428 MAVER1 SU-DHL-2
RCK8
OCILY19
% of proliferating cells
nM
B)
IC50 (nM)
8 19 5 10 5 1 2 3 4 1 2 1 1
ABC-DLBCL GCB-DLBCL MZL MCL ALCL Canine Lymphoma Murine Lymphoma CTCL HL PTCL PLL PMBCL ATCL
C)
48H
72H
% of apoptotic cells compared to DMSO
DMSO 100nM 500nM DMSO 100nM 500nM
D)
REC1
OCILY19
Cell cycle distribution
subG0
G0/G1
S
G2/M
DMSO 500nM 2μM DMSO 500nM 2μM
E)
Healthy donor 1
Healthy donor 2
24h 48h 24h 48h
% of apoptotic cells
DMSO 1μM 10μM DMSO 1μM 10μM DMSO 1μM 10μM DMSO 1μM 10μM

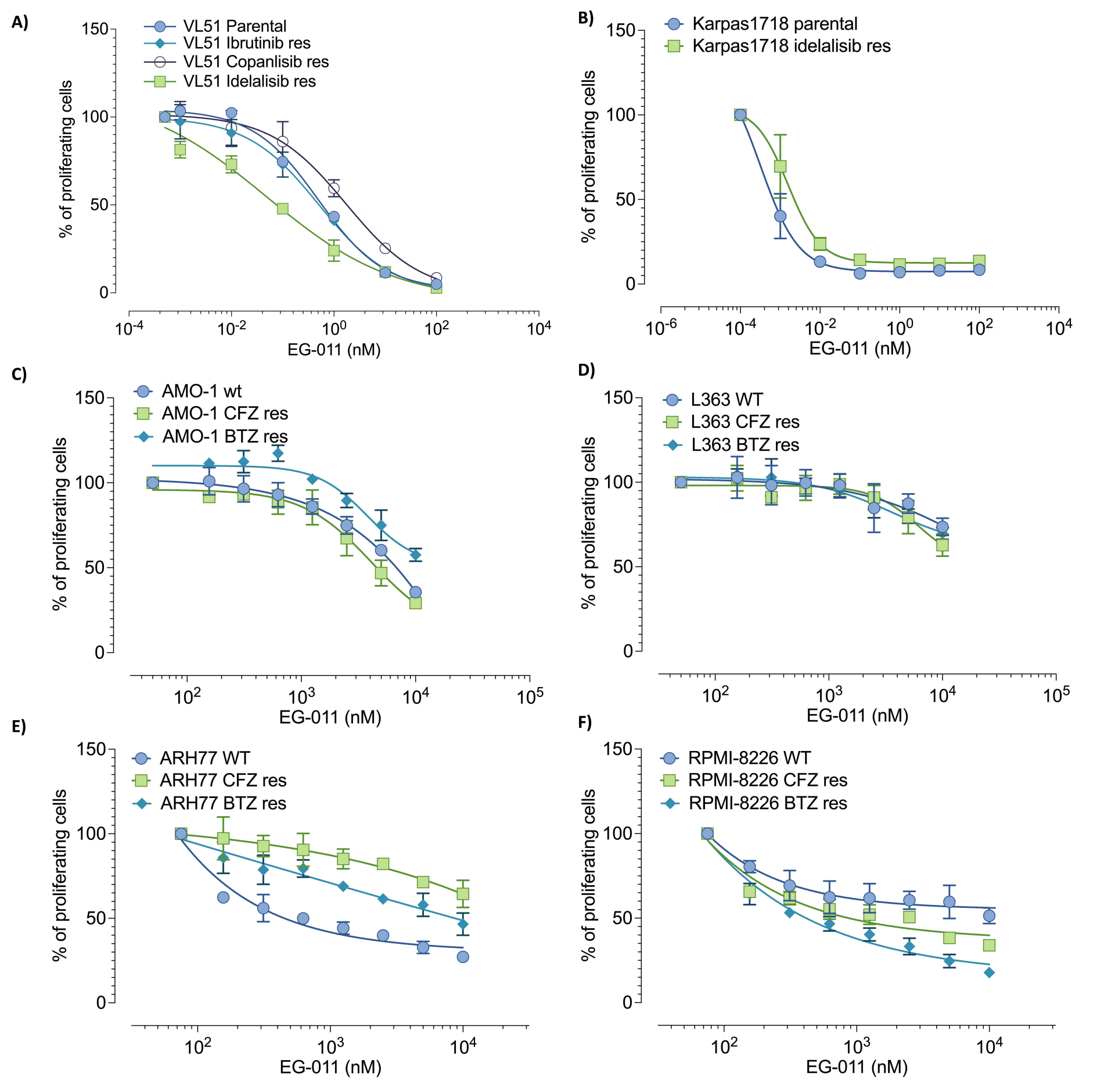
A)
VL51 Parental
VL51 Ibrutinib res
VL51 Copanlisib res
VL51 Idelalisib res
% of proliferating cells
EG-011 (nM)
B)
Karpas1718 parental
Karpas1718 idelalisib res
% of proliferating cells
EG-011 (nM)
C)
AMO-1 wt
AMO-1 CFZ res
AMO-1 BTZ res
% of proliferating cells
EG-011 (nM)
D)
L363 WT
L363 CFZ res
L363 BTZ res
% of proliferating cells
EG-011 (nM)
E)
ARH77 WT
ARH77 CFZ res
ARH77 BTZ res
% of proliferating cells
EG-011 (nM)
F)
RPMI-8226 WT
RPMI-8226 CFZ res
RPMI-8226 BTZ res
% of proliferating cells
EG-011 (nM)

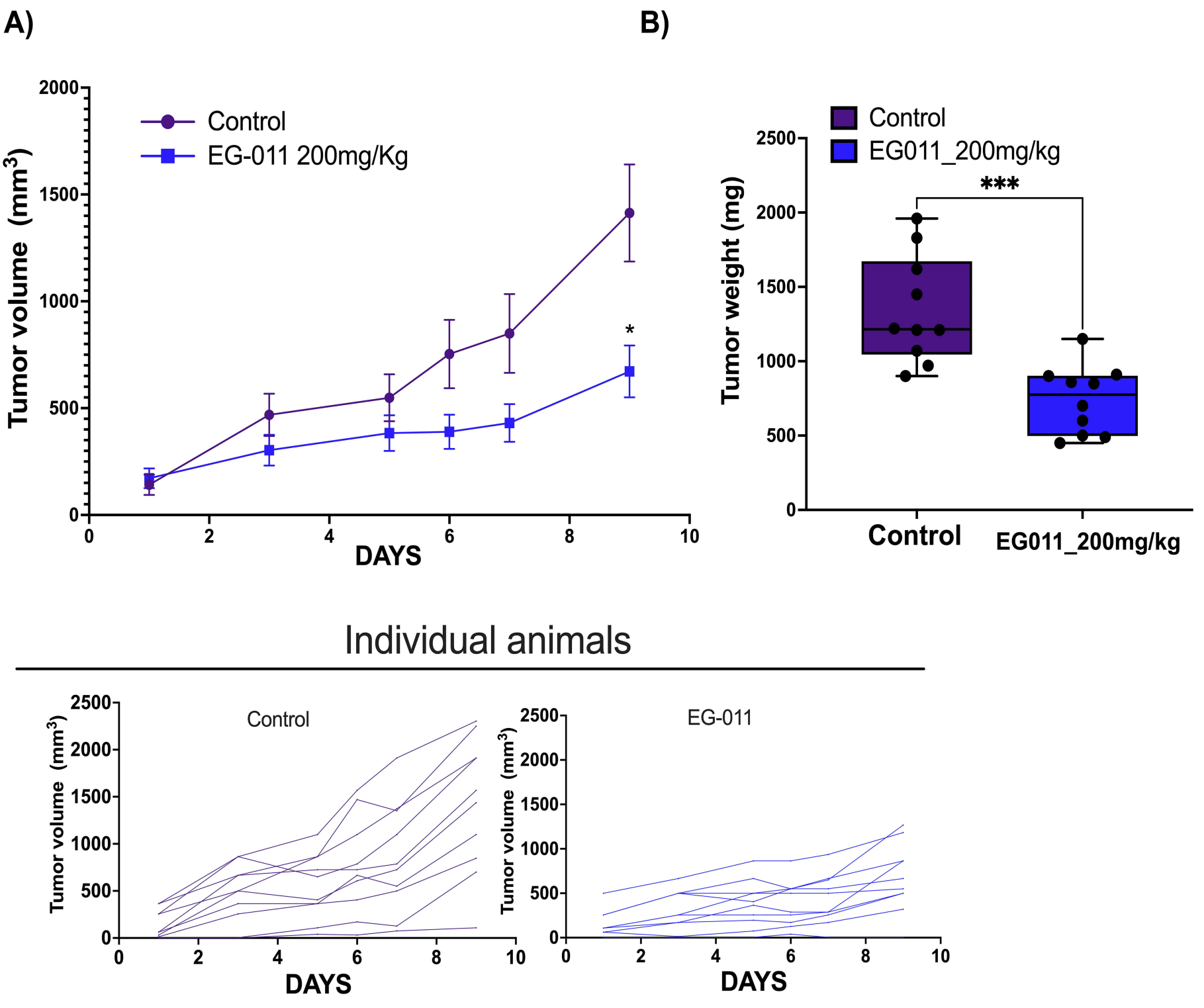
A)
B)
Control
EG-011 200mg/Kg
Tumor volume (mm3)
DAYS
*
Control
EG011_200mg/kg
***
Tumor weight (mg)
Control
EG011_200mg/kg
Individual animals
Control
EG-011
Tumor volume (mm3)
DAYS

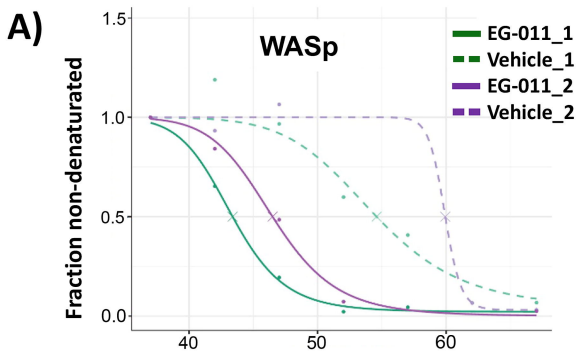
A)
WASp
EG-011_1
Vehicle_1
EG-011_2
Vehicle_2
Fraction non-denaturated
1.5
1.0
0.5
0.0
40
50
60

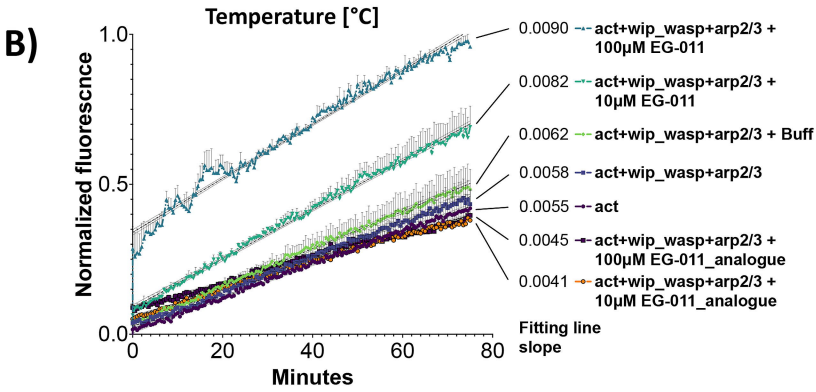
B)
Temperature [°C]
Normalized fluorescnce
1.0
0.5
0.0
0
20
40
60
80
Minutes
0.0090 act+wip_wasp+arp2/3 + 100µM EG-011
0.0082 act+wip_wasp+arp2/3 + 10µM EG-011
0.0062 act+wip_wasp+arp2/3 + Buff
0.0058 act+wip_wasp+arp2/3
0.0055 act
0.0045 act+wip_wasp+arp2/3 + 100µM EG-011_analogue
0.0041 act+wip_wasp+arp2/3 + 10µM EG-011_analogue
Fitting line slope

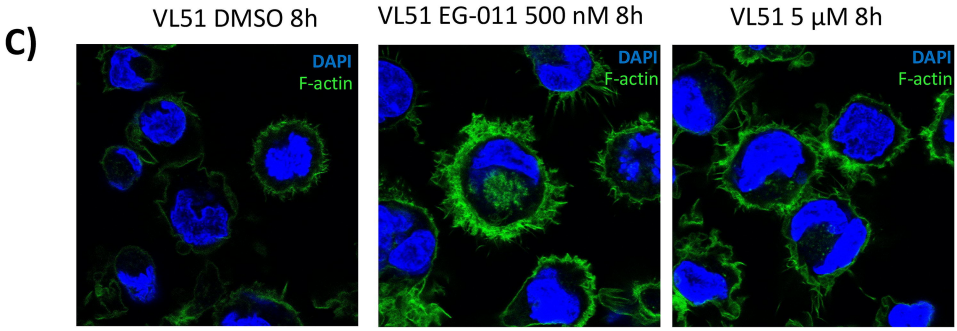
C)
VL51 DMSO 8h
VL51 EG-011 500 nM 8h
VL51 5 µM 8h
DAPI
F-actin

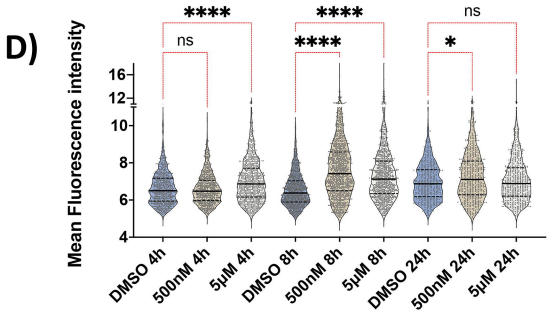
D)
Mean Fluorescence intensity
****
ns
****
****
ns
*
16
12
10
8
6
4
DMSO 4h
500nM 4h
5µM 4h
DMSO 8h
500nM 8h
5µM 8h
DMSO 24h
500nM 24h
5µM 24h

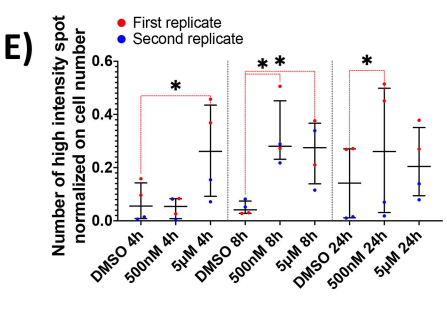
E)
First replicate
Second replicate
Number of high intensity spot normalized on cell number
*
**
*
0.6
0.4
0.2
0.0
DMSO 4h
500nM 4h
5µM 4h
DMSO 8h
500nM 8h
5µM 8h
DMSO 24h
500nM 24h
5µM 24h

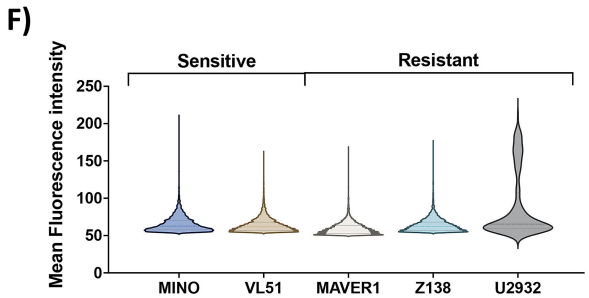
F)
Sensitive
Resistant
Mean Fluorescence intensity
250
200
150
100
50
0
MINO
VL51
MAVER1
Z138
U2932

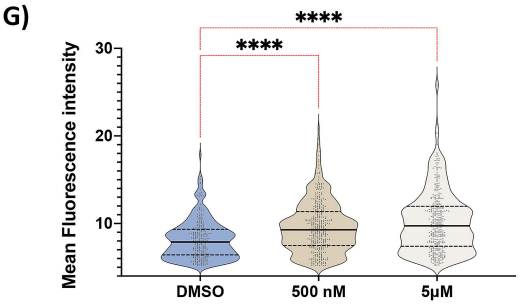
G)
****
****
Mean Fluorescence intensity
30
20
10
DMSO
500 nM
5µM